

# Modeling one-dimensional island growth with mass-dependent detachment rates

R. B. Stinchcombe<sup>1,\*</sup> and F. D. A. Aarão Reis<sup>2,†</sup>

<sup>1</sup> *Rudolf Peierls Centre for Theoretical Physics,  
Oxford University, 1 Keble Road, Oxford OX1 3NP*

<sup>2</sup> *Instituto de Física, Universidade Federal Fluminense,  
Avenida Litorânea s/n, 24210-340 Niterói RJ, Brazil*

(Dated: November 29, 2018)

## Abstract

We study one-dimensional models of particle diffusion and attachment/detachment from islands where the detachment rates  $\gamma$  of particles at the cluster edges increase with cluster mass  $m$ . They are expected to mimic the effects of lattice mismatch with the substrate and/or long-range repulsive interactions that work against the formation of long islands. Short-range attraction is represented by an overall factor  $\epsilon \ll 1$  in the detachment rates (masses  $m \geq 2$ ) relatively to isolated particle hopping rates ( $\epsilon \sim e^{-E/T}$ , where  $E$  is a binding energy and  $T$  is the temperature). We consider various mass-dependences of  $\gamma(m)$ , from rapidly increasing forms such as  $\gamma(m) \sim m$  to slowly increasing ones, such as  $\gamma(m) \sim \left(\frac{m}{m+1}\right)^b$ , with constant  $b$ . A mapping onto a column problem shows that these systems are zero-range processes, whose steady states properties are exactly calculated under the assumption of independent column heights in the Master equation. Simulation provides accurate island size distributions which confirm analytic reductions and are particularly useful whenever the analytical tools cannot provide results in closed form. The shape of island size distributions can be changed from monomodal to monotonically decreasing by tuning the temperature or changing the coverage (one-dimensional density  $\rho$ ). In all cases, small values of the scaling variable  $X \equiv \epsilon^{-1}\rho/(1-\rho)$  favour the monotonically decreasing ones. However, for large  $X$ , rapidly increasing rates  $\gamma(m)$  lead to distributions with peaks very close to  $\langle m \rangle$  and rapidly decreasing tails, while slowly increasing  $\gamma(m)$  provide peaks close to  $\langle m \rangle/2$  and fat right tails.

---

\* E-mail address: r.stinchcombe1@physics.ox.ac.uk

† Email address: reis@if.uff.br

## I. INTRODUCTION

In order to understand the main processes that take place during the growth of thin films and multilayers, it is important to study the initial steps of those processes, i. e. the submonolayer regime. The current belief is that insight derived from the combination of experiment and modeling can lead to better control of nanostructures formed during deposition. Consequently, models of submonolayer growth and coarsening with several types of interactions between the adparticles were intensively studied in the last decades - for a recent review with applications to homoepitaxial growth, see Ref. [1]. Non-equilibrium statistical models are particularly useful for modeling real systems that are confined to long-life metastable states while some atomic processes take place in next-to-equilibrium conditions with the environment.

The recent advances on the production of elongated structures (e. g. nanowires) along step edges of vicinal surfaces [2, 3, 4, 5, 6] and other highly anisotropic growth processes motivated the study of models that produce effectively one-dimensional structures on surfaces under certain conditions [7, 8, 9, 10, 11]. However, in many cases it is advantageous to restrict the processes of particle diffusion and attachment/detachment from islands (possibly competing with the continuous atom deposition) to one spatial dimension, since it enables a more detailed study of the effects of different physico-chemical parameters. One of the interesting problems in this field is to determine the island size distributions under different growth conditions. For instance, recent works have debated the mechanisms responsible for the onset of monomodal or monotonically decreasing distributions in submonolayer growth on vicinal surfaces, since both types of distribution were already observed experimentally [5, 6].

The peaked island size distributions are the most frequently observed in growth on planar surfaces [1] and also appear in some effectively one-dimensional systems [3, 6, 12]. In theoretical models, this feature is observed when some critical island size is assumed, above which there is no further atom detachment. This occurs both for deposition competing with diffusion and for post-deposition coarsening. On the other hand, statistical equilibrium models, where reversibility of attachment and detachment from islands is implicitly assumed, provide monotonically decreasing size distributions in one dimension (more precisely, exponentially decreasing ones) [6, 13].

The simplest reversible non-equilibrium models consider the processes illustrated in Fig. 1a in its one-dimensional version (after deposition has stopped, i. e. with conserved mass) [14, 15, 16, 17, 18]. They account for particle diffusion, aggregation and detachment from islands, with no critical island size. For simplicity, it is assumed that attachment occurs immediately upon contact of a diffusing particle with a cluster, while the detachment occurs with rate  $\gamma(m)$ , where  $m$  is the mass of the cluster from which the particle leaves. Previous work in one-dimension only considered the case of constant  $\gamma$  for all islands ( $m \leq 2$ ) [19], where the steady state presents monotonically decreasing cluster size distributions, similarly to the equilibrium models [6, 13]. The great applicability of the two-dimensional versions of these models explains the small number of studies of the one-dimensional cases.

In this paper, we will consider this class of non-equilibrium one-dimensional models with detachment rates  $\gamma(m)$  increasing with the mass  $m$  of the cluster where the particle is attached. Such dependence is certainly expected in heteroepitaxial growth if small lattice mismatches between the adlayer and the substrate are unfavourable to aggregation of new particles to existing islands. Indeed, the drastic consequences of this feature on island shapes was already illustrated in some systems, such as *Cu* islands on *Ni*(100), where a transition from compact to ramified shapes takes place as the coverage increases [20]. In one-dimensional systems, lattice mismatch is also expected to play a role, although at first approximation the shape effects are not present and the island mass is sufficient to determine the rate for detachment of a bordering atom. The association of a detachment rate with the island size may also be viewed as an alternative to describe the effects of long-range repulsive interactions present in a large number of real systems [21, 22, 23, 24], but which are usually very hard for computation.

The models considered here are equivalent to zero-range processes and do have a factorisable steady state [25, 26]. This feature means that the exact calculation of the steady state properties may be carried out with the use of an independent interval "approximation" (IIA) to the master equation, which implicitly assumes a factorization of probabilities. The IIA, which has already proved to be an exceptional tool to investigate nonequilibrium statistical models [19, 27], here provides exact results for some forms of  $\gamma(m)$ , which are confirmed by numerical simulation data. However, in many cases the latter approach is essential to calculate steady state properties, particularly when average cluster sizes are small and discretization effects play an important role.

We will show that both monomodal and monotonically decreasing cluster size distributions may be obtained in these models depending on the particular form of detachment rate and the coverage. In the analysis of some forms of  $\gamma(m)$  which account for short-range attraction of neighboring atoms (via detachment rates much smaller than isolated particle diffusion coefficients), we will show that it is possible to exchange between those shapes by tuning the temperature or changing the coverage - high temperature and low coverage typically favoring the monotonically decreasing form. Although no quantitative comparison with real systems data will be shown here, we believe that the relative simplicity of our model and the range of qualitative behaviors obtained from it can motivate its use in particular applications. From the theoretical point of view, this work opens the possibility of new applications of the widely studied zero-range processes.

The rest of this work is organized as follows. In Sec. II we present the column picture in which the original problem (Fig. 1) is mapped, the general form of the master equation in the IIA and the method of solution in the steady state. In Sec. III we present the steady state cluster size distributions for selected forms of detachment rates and compare them with results of numerical simulations. We focus on the differences between limiting cases of rapidly and slowly increasing  $\gamma(m)$ . In Sec. IV, we consider systems where formation of small islands is favoured by detachment rates significantly smaller than isolated atom ( $m = 1$ ) diffusion, while  $\gamma(m)$  is increasing. This mimics the competition between short-range attractive and long-range repulsive interactions, a case which may be especially relevant for surface science. In Sec. V we summarize our results and conclusions and discuss possible applications.

## II. PROCESSES, PICTURES, AND GENERAL FORMULATION

As shown in Fig. 1a, the main processes in our problem are: (i) random walk of separated (single) particle, at a rate  $\gamma(1)$ ; (ii) detachment of particle from edge of cluster by particle stepping one unit away from it, at a rate  $\gamma(m)$ , where  $m$  is the cluster mass. In addition, there is (iii) attachment of particle to edge of cluster, occurring immediately after the particle jumps to that position.

The model defined in this so-called cluster picture can also be depicted in a column picture, as illustrated in Fig. 1b. In the latter, the clusters are columns, and the group of  $n$  ( $\geq 1$ ) vacant sites between two adjacent clusters has become a group of  $n - 1$  ( $\geq 0$ ) empty

columns between two filled columns. Thus, one of the vacancies of the cluster picture now acts as a column spacer, and the remaining ones have become columns with  $m = 0$  particles.

This column picture corresponds to a zero-range process [25]. Indeed the mapping just demonstrated achieves the equivalent of the inverse of a mapping from a zero-range process to an exclusion process by other means [25, 28]. In traffic flow models, such as that in Ref. [29], different rates for jumps to the left and to the right must be considered.

The full analytic description of systems with such stochastic processes is provided by the Master equation, which is most easily written in the column picture. The description is simplified by the fact that the process conserves the total particle numbers  $N$ . Thus, using periodic boundary conditions and a total number of sites  $L$  (lattice length in the cluster picture), and denoting by  $N(m)$  the total number of clusters of size  $m$  ( $\geq 1$ ), it follows that (i)  $N = \sum_{m=1}^{\infty} mN(m)$ , (ii) the number of spacers is  $\sum_{m=1}^{\infty} N(m)$ , and (iii)  $N(m)$  equals the number of columns of size  $m$ , for  $m > 0$ . Hence, denoting by  $N(0)$  the number of columns of size zero, we have  $\sum_{m=0}^{\infty} N(m) = L - N \equiv L(1 - \rho)$  (the last step defining the density  $\rho$  in the original picture). Thus the total number of columns (including those of size zero) is constant, as is the density. The system configuration can be specified by the ordered set of numbers of particles in each of the columns in succession:  $(m_1, m_2 \dots) = \{m_i\}$ .

The probability  $P_t\{m_i\}$  at time  $t$  of the configuration  $\{m_i\}$  changes by in and out processes. For example, Fig. 1c shows the process  $(m_1, m_2, m_3, \dots) \rightarrow (m_1 + 1, m_2 - 1, m_3, \dots)$  ( $m_2 \geq 1$ ) having rate  $\gamma(m_2)$ . Collecting the effects of all such processes in a time step  $t \rightarrow t + 1$  gives the full Master equation

$$\begin{aligned}
 P_{t+1}\{m_i\} - P_t\{m_i\} = & \sum_{l=1}^L [\gamma(m_{l-1} + 1) P_t(\dots m_{l-1} + 1, m_l - 1 \dots) \\
 & + \gamma(m_{l+1} + 1) P_t(\dots m_l - 1, m_{l+1} + 1 \dots) \\
 & - 2\gamma(m_l) P_t\{m_i\}] \theta(m_l).
 \end{aligned} \tag{1}$$

The theta function above (zero for  $m \leq 0$ , otherwise unity) is actually redundant as  $P(\dots m - 1 \dots)$  and  $\gamma(m)$  vanish for  $m \leq 0$ .

As an ansatz, one can attempt to find a solution of the Master equation using for  $P_t\{m_l\}$  the factorised form  $\prod_{l=1}^L P_{tl}(m_l)$ . This turns out to give an approximate form (the IIA) for the time-dependent situation, but an exact result for the steady state (the time evolution may be particularly interesting in the case of rates decreasing with cluster mass, and is the subject of our current work). In the special case of homogeneous rates ( $\gamma$  independent

of column position  $l$ ) the steady state Master equation is solved exactly with the function  $P_t(m) = P(m)$ , i. e. independent of  $t$  and  $l$ . Here,  $P(m)$  is the probability that an arbitrarily chosen column has occupancy  $m$ , i. e.  $N(m) / \sum_{m=0}^{\infty} N(m)$ , which corresponds to the probability that a cluster has mass  $m$  in the original problem (Fig. 1a).

The reduced form of the steady state Master equation applying in this simplified (homogeneous) situation can be obtained from Eq. (1) or directly as follows from the processes involved in the evolution of  $P(m)$ . In an appropriately defined time step, the change of  $P(m)$  has positive and negative contributions (from in and out processes)

$$P(m+1)\gamma(m+1)\theta(m) + \delta_{m,0}\gamma(1)P(1) + \Gamma [P(m-1)\theta(m-1) + \delta_{m,1}P(0)] \quad (2)$$

and

$$- P(m)\gamma(m)\theta(m-1) - \delta_{m,1}\gamma(1)P(1) - \Gamma [P(m)\theta(m) + \delta_{m,0}P(0)], \quad (3)$$

respectively, where

$$\Gamma \equiv \sum_{l=1}^{\infty} \gamma(l)P(l). \quad (4)$$

The Master equation for the steady state now reduces to the condition (on  $P(m)$ ) that the sum of contributions of in and out processes (Eqs. 2 and 3) vanishes for each  $m$ . Defining

$$A(m) \equiv P(m)\gamma(m) - \Gamma P(m-1), m \geq 1, \quad (5)$$

that gives the exact relations

$$\begin{aligned} A(1) &= 0, \\ A(m+1) - A(m) &= 0 \quad , \quad m \geq 1, \end{aligned} \quad (6)$$

so that  $A(m)$  vanishes for all  $m \geq 1$ . Thus  $P(m)$  satisfies

$$P(m) = \frac{\Gamma}{\gamma(m)} P(m-1), m \geq 1, \quad (7)$$

yielding

$$P(m) = P(0) \prod_{l=1}^m \frac{\Gamma}{\gamma(l)}, m \geq 1. \quad (8)$$

Direct substitution of the resulting product form for  $P\{m\}$  into the steady state version of the original Master equation (1) verifies that this satisfies it exactly. This result is equivalent to the one [26] previously given for zero-range processes (see e. g. Ref. [25]).

Using the normalization condition

$$\sum_{m=0}^{\infty} P(m) = 1, \quad (9)$$

it can be seen that Eq. (8) is consistent with the definition (4).

Using the definitions of Sec. II, we have

$$\langle m \rangle_{all} \equiv \frac{\sum_{m=0}^{\infty} mN(m)}{\sum_{m=0}^{\infty} N(m)} = \sum_{m=0}^{\infty} mP(m) = \frac{N}{L(1-\rho)} = \frac{\rho}{1-\rho}, \quad (10)$$

where  $\langle m \rangle_{all}$  is the mean cluster size taking into account all columns, including those with zero mass. These equations provide a means to relate  $P(0)$  in Eq. (8) to the density  $\rho$ , as well as the relationship between  $\langle m \rangle_{all}$  and  $\rho$ .

Defining  $\mu \equiv \ln \Gamma$  and

$$\begin{aligned} s(m) &\equiv \sum_{l=1}^m \ln \gamma(l), \quad m \geq 1, \\ s(0) &\equiv 0, \quad m = 0, \end{aligned} \quad (11)$$

and using Eqs. (8) and (9), we find

$$P(m) = \exp [m\mu - s(m)] / \sum_{l=0}^{\infty} \exp [l\mu - s(l)]. \quad (12)$$

From Eq. (10),  $\mu$  can be determined in terms of  $\rho$  by

$$\frac{\rho}{1-\rho} = \sum_{m=0}^{\infty} m \exp [m\mu - s(m)] / \sum_{m=0}^{\infty} \exp [m\mu - s(m)]. \quad (13)$$

The limits in the sums are those appropriate for an infinite system ( $N, L \rightarrow \infty$  at fixed density  $\rho = N/L$ ). The sums are constrained for finite  $L, N$ .

For the infinite system there remains the question whether the sums converge or not. That depends on the form of the rates  $\gamma(m)$  at large  $m$ . In that region  $m$  can be treated as a continuous variable and sums become integrals. This continuum approach is also very useful for  $\rho$  near 1, where typical representative  $m$ 's (such as  $\langle m \rangle_{all}$  in Eq. 10) are large, so typically  $P(m)$  is appreciable at large  $m$ . Using such a continuum approach, it can be seen that for  $\gamma(m)$  increasing with  $m$  at large  $m$  (making  $\ln \gamma(m)$  positive and increasing),  $s(m)$  increases with  $m$  more rapidly than linearly, making the sums in Eqs. (9), (12) and (13) converge, so the steady state solution for  $P(m)$  is physically acceptable:  $P(m)$  decreases with  $m$  at large  $m$  and is typically peaked. This is exactly the situation of interest in real systems where the increase of island size is unfavourable.

In the continuum approach, the location  $m = m_0$  of the peak in  $P(m)$  can be found using

$$0 = \left[ \frac{d}{dm} [\mu m - s(m)] \right]_{m=m_0} = \mu - \ln \gamma(m_0). \quad (14)$$

For  $m_0^2 \gamma'(m_0) / \gamma(m_0) \gg 1$  the peaking is strong, and  $P(m)$  can be approximated by  $\left[ \frac{\gamma(m_0)}{2\pi\gamma'(m_0)} \right]^{1/2} \exp[\mu(m - m_0) - I(m)]$ , where  $I(m) \equiv \int_{m_0}^m \ln[\gamma(l)] dl$ . This has most of its weight in the Gaussian form ( $P(m) \propto \exp[-\frac{1}{2}(\gamma'(m_0)/\gamma(m_0))(m - m_0)^2]$ ), which applies near the peak.

For  $\gamma(m)$  decreasing with  $m$  sufficiently fast at large  $m$ , the sums diverge and there is strictly no steady state in the infinite system. It can be shown that the criterion for no steady state in the infinite system is  $\gamma(m)$  decaying at large  $m$  more slowly than a constant times  $1 + \frac{2}{m}$  [25]. In this case, the system will coarsen forever, but such situations [ $\gamma(m)$  decreasing with  $m$ ] will not be considered here.

### III. STEADY STATE BEHAVIOR FOR SELECTED DETACHMENT RATES

In this Section, analytic predictions and simulation results for steady state properties will be presented and compared. The emphasis will be on the empirically realistic "thermodynamic" limit of very large systems, in which steady states are achievable. The steady state properties to be discussed here are the cluster size distributions and the average cluster sizes. However, it is important to mention that, from now on, cluster sizes are defined by averaging only over masses  $m \geq 1$ , in contrast with Eq. (10), which also took into account columns with zero mass. This new average will be denoted  $\langle m \rangle$ , and provides a more appropriate physical description of the system in the original cluster picture. Indeed, except where explicitly indicated, we will refer to that original picture in the following.

The simulations were typically performed in lattices of sizes  $L = 8192$ , with several densities and different forms of  $\gamma(m)$ . Due to the small cluster sizes imposed by the system dynamics, in all cases finite-size effects are negligible (this was checked by comparison of results in different lattice sizes). The generation of a sequence of configurations begins with the deposition of a random layer of density  $\rho$ . Subsequently, the dynamics with diffusion, attachment and detachment processes is allowed, and the evolution of the cluster size distribution is monitored. Typically, it is assumed that the steady state is attained if no appreciable change (e. g. 1% in the peak) is found in the distribution at the last time decade

of the simulation, after averaging over at least 100 initial configurations (i. e. 100 different sequences). Under these conditions, the representative configurations are attained, on the average, after 100 – 1000 detachments of particles aggregated to small clusters. Anyway, it is important to note that in our models steady state properties are independent of the initial system configuration, thus the same results would be obtained if diffusion and detachment processes were competing with deposition during the production of the first configuration with the desired density  $\rho$  (however, there are special models where steady state properties depend on the initial configuration - see e. g. Ref. [32]).

First we consider the case (i) of constant detachment rate,  $\gamma(m) = a$  for  $m \geq 2$  and isolated particle hopping rate  $\gamma(1) = b$ . The analysis proceeding from Eqs. (13) and (12) gives a size distribution which is exponentially decreasing in  $m$  for  $m \geq 2$ . For the special case  $b = a$ , using  $s(m) = m \ln a$ , we have  $P(m) = (1 - \rho) \rho^m$  for all  $m$ . Such results were formerly predicted in Ref. [19] and numerically confirmed in Ref. [30]. These distributions are equivalent to those obtained in equilibrium (reversible) models with nearest neighbor interactions between the adatoms [6, 13].

Now we consider the power law case (ii),  $\gamma(m) = m^k$  for  $m \geq 1$ , in which the reduction of the analytic result (12) for  $P(m)$  is less straightforward than in the previous case. For this reason, most results are obtained from simulation. In Fig. 2, we show the scaled distributions for  $k = 1$  and densities  $\rho = 0.5$ ,  $\rho = 0.75$  and  $\rho = 0.95$  (in this and subsequent plots, dashed curves are guides to the eye). For small and medium densities, isolated particles ( $m = 1$ ) are predominant and the distribution is rapidly decreasing, so that it seems to decay faster than a simple exponential for  $\rho \lesssim 0.5$ . As the coverage increases, it crosses over to a peaked (monomodal) distribution, which becomes very sharp for  $\rho$  close to 1. This crossover is directly related to the increase in the average size  $\langle m \rangle \approx \rho / (1 - \rho)$ , from a value near unity for small  $\rho$  (where the decrease is monotonic) to large values for large  $\rho$  (where the peak is close to  $\langle m \rangle$ ).

The analytical distribution of case (ii) becomes simple for  $\rho \approx 1$ , since there the typical masses are large and continuum approximations can be used. That results in  $P(m) \propto \exp [(\mu + k)m - km \ln m]$  ( $m$  large). For  $k = 1$ , this is the large  $m$  approximation to a Poisson distribution. The agreement with simulation results is illustrated in the inset of Fig. 2 for  $k = 1$  and  $\rho = 0.95$ , where  $\log [P(m)]$  is shown to be a function of  $m \ln(m) - Cm$ , with a fitting constant  $C = 3.92$ .

We next consider another simple detachment rate function,  $\gamma(m) = \left(\frac{m}{m+1}\right)^b$  for  $m \geq 1$ , hereafter called case (iii). The main difference from case (ii) is the fact that  $\gamma$  does not diverge as  $m \rightarrow \infty$ . Using Eqs. (13) and (12), we obtain exactly  $P(m) \propto (m+1)^b \exp(-\beta m)$ , with  $\beta$  constant. For low integer values of  $b$ , the constant  $\beta$  and the normalization constant can easily be obtained analytically in terms of the density. For the simplest case  $b = 1$ , we obtain  $\beta = \ln\left(\frac{2-\rho}{\rho}\right)$  and  $\langle m \rangle = \frac{(2-\rho)^2}{(1-\rho)(4-3\rho)}$ . We remark here that the case  $b = -2$  is marginal: from the discussion at the end of Sec. II (see also Ref. [25]), the infinite system achieves a steady state if  $b \geq -2$  but not if  $b < -2$ .

In Fig. 3 we show the scaled cluster size distributions for case (iii) obtained from simulation, with  $b = 1$  and coverages  $\rho = 0.5$  and  $\rho = 0.9$ . Both show excellent agreement with the analytical results (hereafter represented by solid curves in the plots). Again we observe that the distribution is monotonically decreasing for small coverages, where  $\langle m \rangle$  is close to 1, while for larger coverages there appears a peak. However, there is an important difference from case (ii) here: instead of having a sharp peak close to  $\langle m \rangle$ , the distribution for large coverages has a very fat left tail and the most probable island size may be smaller than  $\langle m \rangle/2$  (see data for  $\rho = 0.9$  in Fig. 3). This difference is certainly a consequence of the slower increase of the detachment rate with the cluster mass.

We also analyzed other forms of detachment rates, namely simple exponential, logarithmic  $\gamma(m)$ , and the particular logarithmic case  $\gamma(m) = c[\ln(m+1)]^{[1+\ln(m+1)]}$ , for which a closed analytical form of  $P(m)$  can be obtained. In all cases, the analytically predicted distributions agree very well with simulation data. With the logarithmic forms, the qualitative behavior is intermediate between cases (ii) and (iii) above.

The peaked cluster size distributions shown above were always obtained for large densities. At first sight, this condition seems to be unattainable in experiments on submonolayers on vicinal surfaces, since the one-dimensional character of the adlayer (e. g. chain-like structures along the step edges) is lost at high coverages. However, in Sec. IV, we will show that under certain realistic conditions on  $\gamma(m)$ , it is also possible to observe peaked distributions for densities lower than 0.5.

Moreover, it is important to stress that the density  $\rho$  of particles along the steps can be much larger than the nominal coverage  $\theta$  of the surface because the latter is an adatom density per substrate area, while  $\rho$  is the filling of one-dimensional rows. As an example, we refer to the STM image of *Ag* deposited on *Pt(997)* in Fig. 1b of Ref. [6]), where the

coverage  $\theta = 0.04$  monolayers is much smaller than the effective filling  $\rho \approx 0.3$  of the step rows.

#### IV. SYSTEMS WITH COMPETING INTERACTIONS AND TEMPERATURE EFFECTS

Here we extend the study of Sec. III to systems with the mass-dependent detachment rates all far less than the isolated atom diffusion rate  $\gamma(1)$ , by an overall factor  $\epsilon \sim \exp(-E/k_B T) \ll 1$ . Here,  $E$  may be interpreted as a binding energy between neighboring adatoms, and  $T$  is the temperature (see e. g. the discussion on the diffusivities for initial state interactions in Ref. [31], where only short-range interactions were considered). For low temperatures, that factor significantly reduces the mobility of aggregated atoms when compared to the isolated ones. On the other hand, the mass dependence of  $\gamma$  accounts for the effects of the interactions with the substrate, which works against the increase of cluster size (e. g. effects of lattice mismatch or substrate-mediated repulsive interactions). We will typically work with  $10^{-1} \leq \epsilon \leq 10^{-3}$  for each form of  $\gamma(m)$ , in order to show the possible effects of the temperature in the island size distributions. Simulation work here will focus on low coverages, typically below or at half filling of the one-dimensional rows.

First we consider the generalization of case (ii), where  $\gamma(m) = c(m) m^k$  with  $c(1) = 1$ , and  $c(m) = \epsilon \ll 1$  for  $m \geq 2$ . This means that detachment rates from small clusters (up to masses  $\approx \epsilon^{-1}$ ) are smaller than the isolated atom diffusion rate, but larger clusters are very unstable.

For  $k = 1$ , no simple closed form for the cluster size distribution can be obtained. In Figs. 4a and 4b we show the simulation results with densities  $\rho = 0.1$  and  $\rho = 0.5$ , respectively. In both plots we consider  $\epsilon = 10^{-2}$  and  $\epsilon = 10^{-3}$ . For low density (Fig. 4a), the distributions are monotonically decreasing up to  $\epsilon \sim 10^{-2}$ , but a peak at small  $m$  appears at sufficiently low temperatures (i. e. very small  $\epsilon$ ). For medium density, Fig. 4b shows that the temperature does not need to be so small for the onset of a peaked distribution: the peak is present for  $\epsilon = 10^{-2}$  and it is well defined at  $\epsilon = 10^{-3}$ . These results must be compared with those in Fig. 2 for  $k = 1$  and  $\rho = 0.5$ , but  $\epsilon = 1$ , where the distribution is monotonically and rapidly decreasing.

Analytical results can be obtained for the generalized case (ii) only for  $k < 1$  and  $\epsilon \ll 1$ ,

where average cluster sizes are large and a continuum approximation of the cluster size distribution is possible. In these conditions, we have  $P(m) \propto \frac{1}{(m!)^k} \left\{ \frac{1}{k} \ln [B/(\ln B)^\zeta] \right\}^{km}$ , with  $B \equiv \frac{k^{2-k/2}}{(2\pi)^{(1-k)/2}} \frac{\rho}{\epsilon(1-\rho)}$  and  $\zeta = \frac{3-k}{2}$ . This is a monomodal distribution with  $\langle m \rangle \approx \frac{1}{k} \ln [B/(\ln B)^\zeta]$ , which confirms the general trend that this shape is favoured by large densities and small temperature (small  $\epsilon$ ).

Unfortunately, the above formula for  $P(m)$  is accurate only for very small  $\epsilon$  and very small  $k$ , otherwise the continuum approximation fails due to the discreteness of the typical cluster sizes and the large statistical weight of isolated particles. As an example, we compare in Fig. 5a and 5b the analytical and numerical cluster size distributions for  $k = 1/2$  and  $\rho = 0.5$ , with  $\epsilon = 10^{-2}$  and  $\epsilon = 10^{-3}$ , respectively. Even for  $\epsilon = 10^{-3}$ , where  $\langle m \rangle \approx 7$ , we observe deviations of the analytical approximation from the numerical data.

The results in Figs. 4 and 5, as well as the analytical approximation for  $k < 1$  and  $\epsilon \ll 1$ , show another important feature: the peaks of the distributions are very close to  $\langle m \rangle$ , similarly to the case (ii) with  $\epsilon = 1$  studied in Sec. III. We recall that these are cases of rapidly increasing  $\gamma(m)$ , in which the formation of large clusters is highly unfavourable.

Now we consider the generalization of case (iii), where  $\gamma(m) = c(m) \left( \frac{m}{m+1} \right)^b$ , with  $c(1) = 1$ , and  $c(m) = \epsilon$  for  $m \geq 2$ . The resulting probability distribution  $P(m)$  is of the same form as the one in Sec. III (i. e. for the special case  $\epsilon = 1$ ), however the small  $\epsilon$  gives much lower weight to  $P(m)$ ,  $m \geq 1$ , than  $P(0)$ , and the peak of the distribution is, for most densities, pushed out to much larger masses. For general  $b$  it is possible to show that for small enough  $\epsilon$  (very much less than both  $\rho$  and  $(1-\rho)^{b+1}$ ) the mean cluster size has the form  $\langle m \rangle \sim \left[ \frac{\rho}{\epsilon(1-\rho)} \frac{(b+1)^{b+1}}{b!} \right]^{1/(b+2)}$ .

In Figs. 6a-d we show the simulation results for  $b = 1$ , with densities  $\rho = 0.1$  and  $\rho = 0.5$  and detachment factors  $\epsilon = 10^{-2}$  and  $\epsilon = 10^{-3}$ . For this value of  $b$ , the full distribution can be obtained analytically as  $P(m) \propto (m+1) e^{-\beta m}$ ,  $\beta = \left( \frac{2\epsilon(1-\rho)}{\rho} \right)^{1/3}$ . It compares well with simulation data for intermediate densities and small values of  $\epsilon$ , as shown in Fig. 6b.

Lowering the temperature also provides peaked distributions in this case, and the position of the peak is shifted to larger masses as the density increases. The effect of temperature is important only in the right tail of the distribution, which typically has a small number of data points, corresponding to small islands. Similarly to what was observed in Sec. III, the peaks are located close to  $\langle m \rangle/2$  and the left tail is very fat. This is a signature of a weak size-dependence of the detachment rates. However, the main difference from the results in

Sec. III is again the possibility of finding the transition from a monotonically decreasing distribution to a monomodal one by tuning the temperature, with a coverage not too large.

For the general case of rate functions  $\gamma(m)$  increasing with  $m$  (at large  $m$ ), the mean cluster size  $\langle m \rangle$  can always be made large at low densities by suppressing detachment rates by a suitably small factor  $\epsilon$ , compared to the diffusion rate  $\gamma(1)$ . Considering  $\gamma(m) = \epsilon\nu(m)$  for  $m \geq 2$  and  $\gamma(1) = \nu(1)$ , the relationships

$$\langle m \rangle \sim F(X) \quad , \quad X \equiv \frac{\rho}{\epsilon(1-\rho)} \quad (15)$$

of average cluster size to density and Arrhenius rate parameter  $\epsilon$  which result at small  $\epsilon$  for a variety of detachment rate functions (at large  $m$ ) are:

$$\begin{aligned} \nu(m) = m^k &\Rightarrow F(X) = \frac{1}{k} \ln X, \\ \nu(m) = (\ln m)^{\alpha \ln m} &\Rightarrow F(X) = \frac{\ln X}{\alpha \ln \ln \ln X}, \\ \nu(m) = [me^{(\ln m)^2}]^\alpha &\Rightarrow F(X) = \frac{\ln X}{\alpha \ln \ln X}, \\ \nu(m) = e^{\alpha m^n} &\Rightarrow F(X) = \left[ \frac{n+1}{\alpha n} \ln X \right]^{1/(n+1)}. \end{aligned} \quad (16)$$

It can be seen that the effect of  $\epsilon$  (in reducing the density required to get a large mean cluster mass) diminishes as the rate of increase of  $\nu$  with  $m$  increases. More importantly, these results show that density and temperature control the island size distribution through the scaling variable  $X$ , so that monomodal (monotonically decreasing) forms are found for large (small)  $X$ .

## V. DISCUSSION AND CONCLUSION

We studied one-dimensional models of island formation by diffusion, attachment and detachment of single particles, considering detachment rates  $\gamma$  increasing with the island mass  $m$ . This type of model may be of experimental interest because it can be used to simplify the description of more complex interactions that prevent the formation of large atomic islands. Indeed, these models are equivalent to zero-range processes in which the system attains a steady state. An independent interval "approximation" to the Master equation was proposed in order to calculate the cluster size distribution which actually provides an exact description in the steady state. The tools necessary for derivation of

explicit distributions for any particular form of  $\gamma(m)$  were provided and results for a variety of cases were presented and compared with numerical simulation data.

The representative rate functions analyzed above include some which arise from associating (Arrhenius) detachment rates with potentials  $U(m)$  for particles at the end of a cluster of size  $m$ .  $U(m)$  is then a sum, from  $l = 1$  to  $m - 1$ , of pair potentials  $V(l)$  for separation  $l$ . The forms  $V$  vanishing,  $V$  Coulomb-like and inverse square then give (exactly in the first two cases, and for large  $m$  in the third one) the detachment rate functions of cases (i), (ii), (iii), respectively. In addition, we also mimicked the presence of short-range attraction in the models where the detachment rates were smaller than isolated particle hopping rates by an overall factor  $\epsilon \ll 1$ .

One of the important conclusions of this work is the possibility of changing the shape of island size distributions, from monomodal to monotonically decreasing ones, by tuning the temperature or changing the coverage. For different forms of detachment rates (rapidly or slowly decreasing with  $m$ ), it was shown that high temperatures and low coverages are favourable for the onset of the monotonically decreasing distributions, their combined effect being described by the scaling variable  $X \equiv \frac{\rho}{\epsilon(1-\rho)}$ . This transition is not usual in non-equilibrium modeling of submonolayer growth, particularly when irreversible attachment to islands (i. e. a critical island size) is assumed. However, it is an important finding because both shapes of distribution were already observed (isolated) in island growth near step edges of vicinal surfaces [5, 6].

On the other hand, rapidly or slowly increasing  $\gamma(m)$  have different effects on the position of the peak of the island size distributions and on its right tail. Rapidly increasing  $\gamma(m)$  [e. g. case (ii) above] lead to peaks very close to  $\langle m \rangle$  and rapidly decreasing tails, since formation of large clusters is very difficult. However, the slowly decreasing  $\gamma(m)$  forms [e. g. case (iii), where  $\gamma(m)$  does not diverge when  $m \rightarrow \infty$ ] provide peaks close to  $\langle m \rangle / 2$  and fat right tails. In real systems where island size distributions are measured, these results may give clues on how intense are the mechanisms that work against the formation of large clusters.

Despite the fact that no application to a particular real system was proposed here, we believe that the framework developed in this paper may be useful for such applications. Long range interactions frequently play a role in submonolayer growth but introduce difficulties to both analytical (scaling) and numerical calculations, even when they are limited to one

dimension (see. e. g. [33]). Consequently, the inclusion of simpler mechanisms in a model system may be useful, such as the association of detachment rates to the full cluster size suggested here. The fact that our model corresponds to a zero-range process allows for much simpler analytical calculations of steady state properties, in contrast to other (not less important) approaches, such as the introduction of energy barriers for particle attachment to clusters [23, 34]. Finally, it is also interesting to recall that gas adsorption in carbon nanotubes may be viewed as a one-dimensional clustering problem, thus it is another field where this type of non-equilibrium model may find application. Indeed, simple statistical equilibrium models of interacting particles in finite lattices were already proposed for those systems [35].

### Acknowledgments

We wish to thank Dr. Rosemary Harris for a discussion concerning zero-range process results for finite systems.

FDAA Reis thanks the Rudolf Peierls Centre for Theoretical Physics of Oxford University, where this work was done, for hospitality, and acknowledges support by the Royal Society of London (UK) and Academia Brasileira de Ciências (Brazil) for his visit.

RB Stinchcombe acknowledges support from the EPSRC under the Oxford Condensed Matter Theory Grants, numbers GR/R83712/01, GR/M04426 and EP/D050952/1.

- 
- [1] J.W. Evans, P. A Thiel, M. C. Bartelt, *Surface Science Reports* **61**, 1 (2006).
  - [2] F.J. Himpsel, A. Kirakosian, J. N. Crain, J. L. Lin, and D. Y. Petrovykh, *Solid State Communications* **117**, 149 (2001).
  - [3] P. Gambardella, M. Blanc, H. Brune, K. Kuhnke, and K. Kern, *Phys. Rev. B* **61**, 2254 (2000).
  - [4] Z. Gai, G. A. Farnan, J. P. Pierce and J. Shen, *App. Phys. Lett.* **81**, 742 (2002).
  - [5] M. A. Albao, M. M. R. Evans, J. Nogami, D. Zorn, M. S. Gordon and J. W. Evans, *Phys. Rev. B* **72**, 035426 (2005).
  - [6] P. Gambardella, H. Brune, K. Kern, and V. I. Marchenko, *Phys. Rev. B* **73**, 245425 (2006).
  - [7] Y. W. Mo, J. Kleiner, M. B. Webb, and M. G. Lagally, *Phys. Rev. Lett.* **66**, 1998 (1991).

- [8] K. I. Mazzitello, J. L. Iguain, and H. O. Martin, *J. Phys. A* **32**, 4389 (1999).
- [9] Y. Li, M. C. Bartelt, J. W. Evans, N. Waelchli, E. Kampshoff, and K. Kern, *Phys. Rev. B* **56**, 12539 (1997).
- [10] R. Ferrando, F. Hontinfinde, and A. C. Levi, *Phys. Rev. B* **56**, R4406 (1997).
- [11] J. B. Taylor and P. H. Beton, *Phys. Rev. Lett.* **97**, 236102 (2006).
- [12] V. Repain, G. Baudot, H. Ellmer, and S. Rousset, *Mater. Sci. Engineering B* **96**, 178 (2002).
- [13] V. I. Tokar and H. Dreyssé, *Phys. Rev. B* **74**, 115414 (2006).
- [14] S. Clarke and D. D. Vvedensky, *J. Appl. Phys.* **63**, 2272 (1988).
- [15] H. Brune, *Surf. Sci. Rep.* **31**, 121 (1998).
- [16] T. Ala-Nissila, R. Ferrando, and S. C. Ying, *Adv. Phys.* **51**, 949 (2002).
- [17] C. Ratch and J. A. Venables, *J. Vac. Sci. Technol. A* **21**, S96 (2003).
- [18] M. Biehl, *arXiv:cond-mat/0406707* (2004).
- [19] F. D. A. Aarão Reis and R. B. Stinchcombe, *Phys. Rev. E* **70**, 036109 (2004).
- [20] B. Müller, L. Nedelmann, B. Fischer, H. Brune, J. V. Barth, and K. Kern, *Phys. Rev. Lett.* **80**, 2642 (1998).
- [21] A. Bogicevic, S. Ovesson, P. Hyldgaard, B. I. Lundqvist, H. Brune and D. R. Jennison, *Phys. Rev. Lett.* **85**, 1910 (2000).
- [22] S. Ovesson, *Phys. Rev. Lett.* **88**, 116102 (2002).
- [23] J. A. Venables and H. Brune, *Phys. Rev. B* **66**, 195404 (2002).
- [24] G. Nandipati and J. G. Amar, *Phys. Rev. B* **73**, 045409 (2006).
- [25] M. R. Evans and T. Hanney, *J. Phys. A: Math. Gen.* **38**, R195 (2005).
- [26] F. Spitzer, *Adv. Math.* **5**, 246 (1970).
- [27] S. N. Majumdar, S. Krishnamurthy, and M. Barma, *Phys. Rev. Lett.* **81**, 3691 (1998).
- [28] M. Kanai, *J. Phys. A: Math. Theor.* **40**, 7127 (2007).
- [29] J. Kaupuzs, R. Mahnke, and R. J. Harris, *Phys. Rev. E* **72**, 056125 (2005).
- [30] A. Chame and F. D. A. Aarão Reis, *Physica A* **376**, 108 (2007).
- [31] S. H. Payne and H. J. Kreuzer, *Phys. Rev. B* **75**, 115403 (2007).
- [32] M. Barma, M. D. Grynberg, and R. B. Stinchcombe, *Phys. Rev. Lett.* **70**, 1033 (1993).
- [33] H. S. Ammi, A. Chame, M. Touzani, A. Benyoussef, O. Pierre-Louis, and C. Misbah, *Phys. Rev. E* , **71** 041603 (2005).
- [34] D. Kandel, *Phys. Rev. Lett.* **78**, 499 (1997).

[35] M. Hodak and L. A. Girifalco, Phys. Rev. B **64**, 035407 (2001).

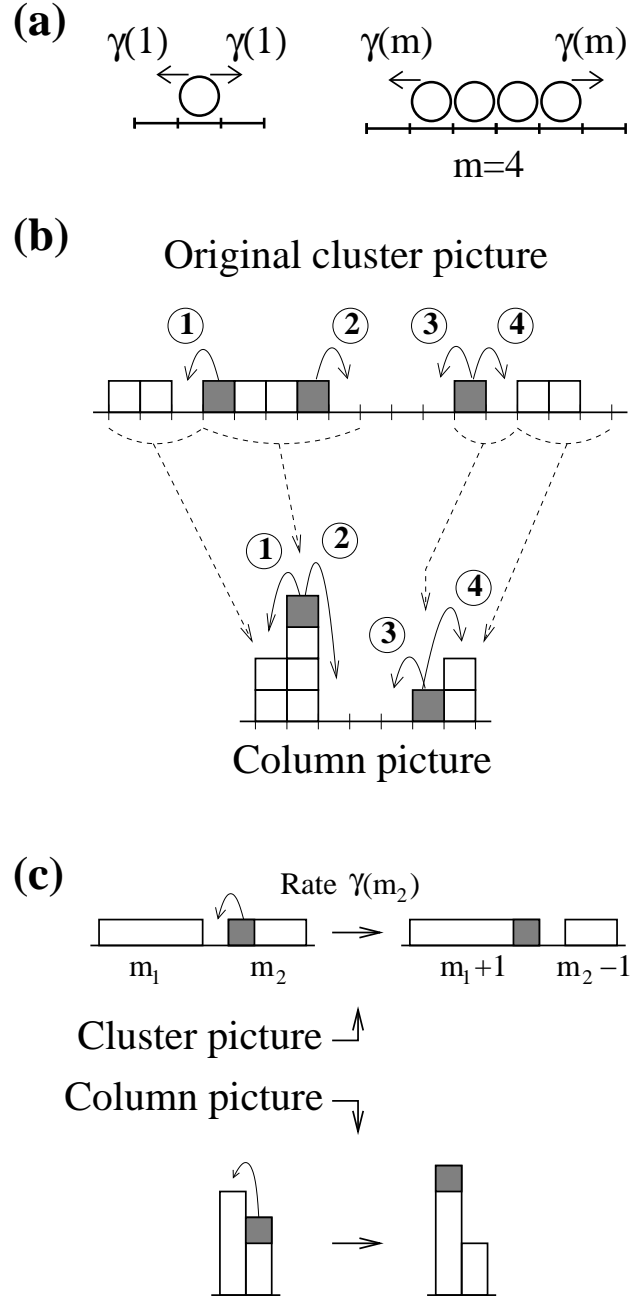


FIG. 1: (a) Illustration of the diffusion ( $m = 1$ ) and detachment ( $m > 1$ ) processes of the model, with the associated rates  $\gamma(m)$ . (b) Examples of detachment processes (1,2) and hopping processes (3,4) of filled particles, in the original cluster picture and in the corresponding column picture. Dashed lines show the correspondence between clusters in the two pictures. (c) Example of leftward movement of an aggregated particle.

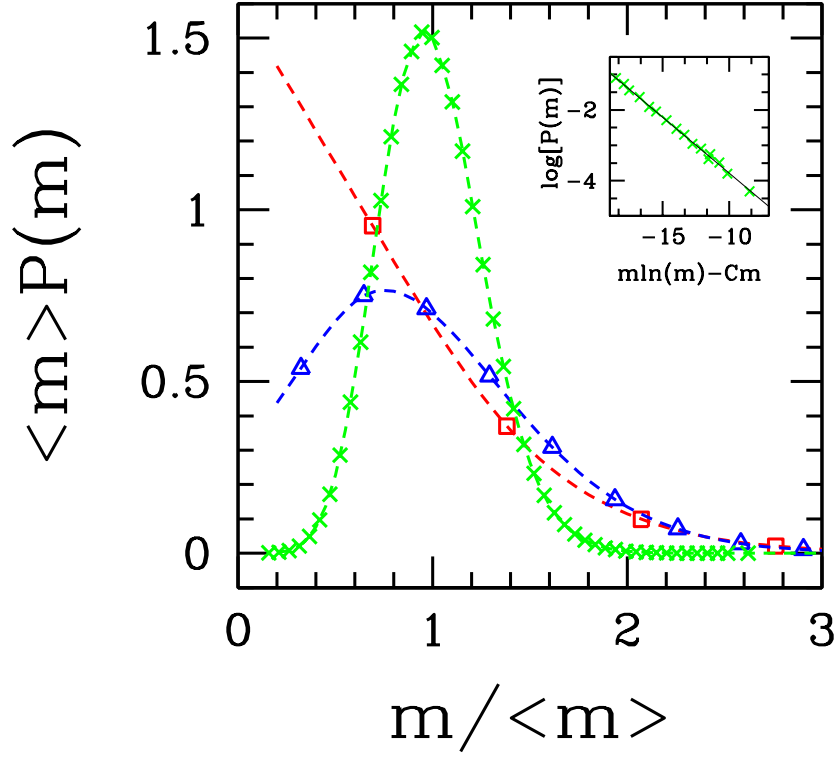


FIG. 2: (Color online) Scaled cluster mass distribution for detachment rate  $\gamma(m) = m$  (case (ii) with  $k = 1$ ), with densities  $\rho = 0.5$  (squares),  $\rho = 0.75$  (triangles) and  $\rho = 0.95$  (crosses). Dashed curves are drawn to guide the eye. Inset: the rescaled data for  $\gamma(m) = m$  and  $\rho = 0.95$ , with a fitting constant  $C = 3.92$ , is consistent with a Poisson distribution (the solid line is a linear fit of the data).

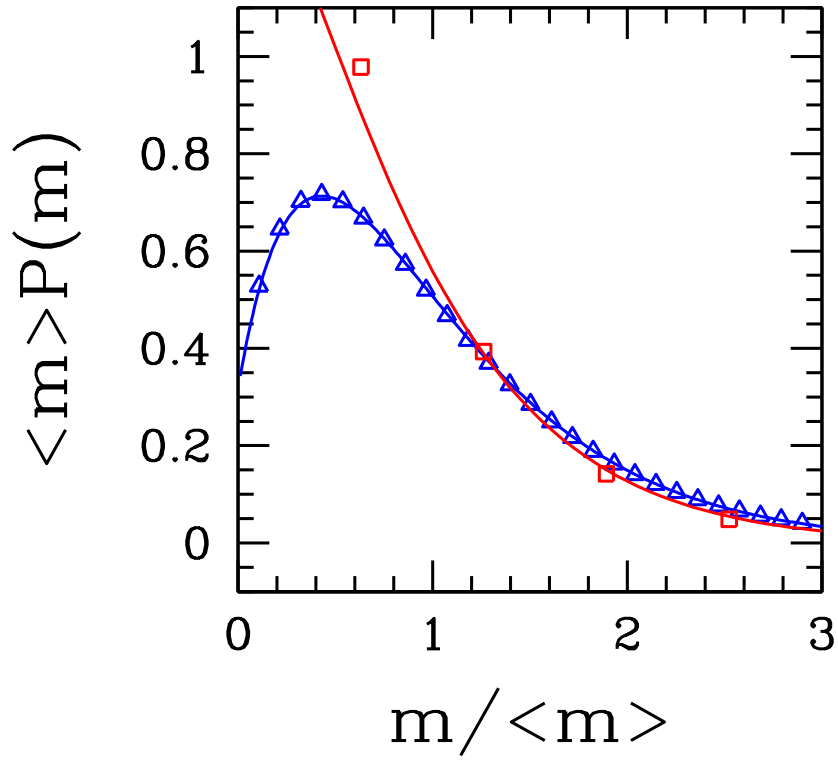


FIG. 3: (Color online) Scaled cluster mass distribution obtained from simulation for detachment rate  $\gamma(m) = m/(m + 1)$  [case (iii)] with densities  $\rho = 0.5$  (squares) and  $\rho = 0.9$  (triangles). Solid curves are the corresponding analytical results.

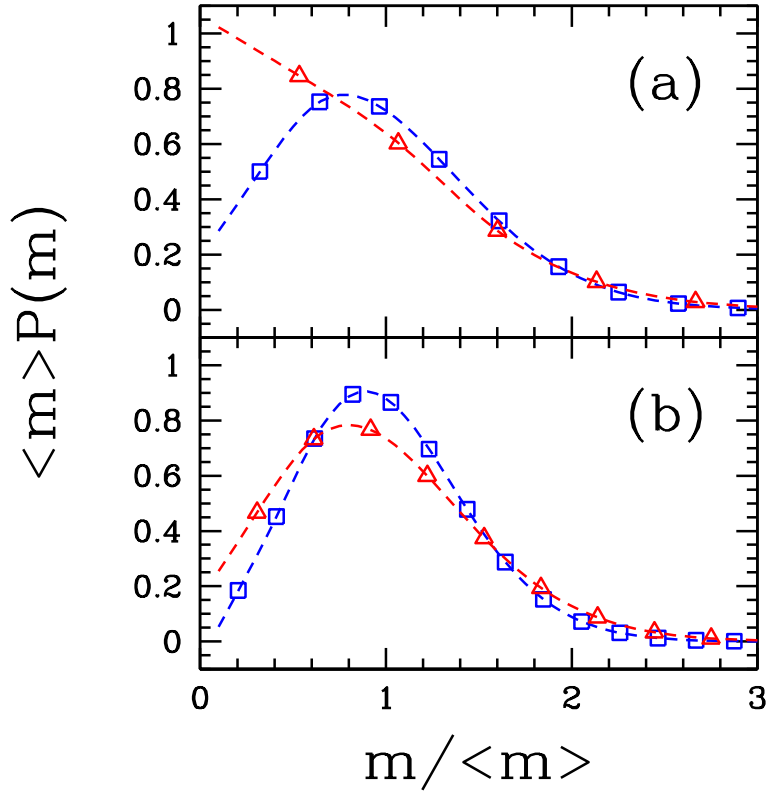


FIG. 4: (Color online) Scaled cluster mass distributions obtained from simulation for detachment rate  $\gamma(m) = c(m)m$ , with  $c(1) = 1$  and  $c(m) = \epsilon$  for  $m \geq 2$ , and densities (a)  $\rho = 0.1$  and (b)  $\rho = 0.5$ . In both panels,  $\epsilon = 10^{-2}$  (triangles) and  $\epsilon = 10^{-3}$  (squares). Dashed curves are drawn to guide the eye.

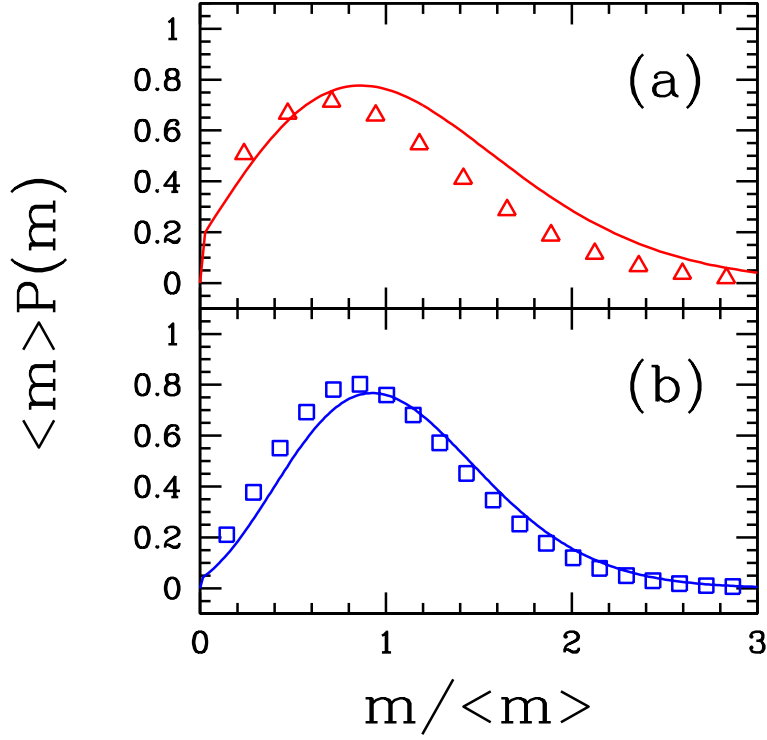


FIG. 5: (Color online) Scaled cluster mass distributions for detachment rate  $\gamma(m) = c(m)m^{1/2}$ , with  $c(1) = 1$  and  $c(m) = \epsilon$  for  $m \geq 2$ , density  $\rho = 0.5$  and (a)  $\epsilon = 10^{-2}$  and (b)  $\epsilon = 10^{-3}$ . Symbols indicate simulation data and solid curves show the corresponding analytical results in the continuum approximation.

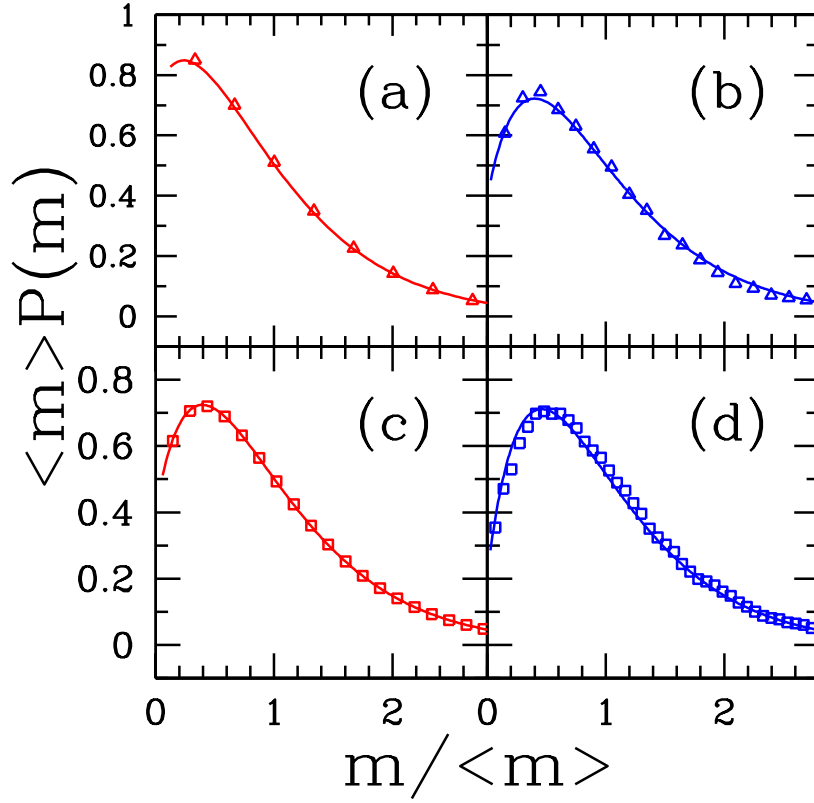


FIG. 6: (Color online) Scaled cluster mass distributions for detachment rate  $\gamma(m) = c(m)m/(m+1)$ , with  $c(1) = 1$  and  $c(m) = \epsilon$  for  $m \geq 2$ , and: (a)  $\rho = 0.1$ ,  $\epsilon = 10^{-2}$ ; (b)  $\rho = 0.1$ ,  $\epsilon = 10^{-3}$ ; (c)  $\rho = 0.5$ ,  $\epsilon = 10^{-2}$ ; (d)  $\rho = 0.5$ ,  $\epsilon = 10^{-3}$ . Symbols indicate simulation data and solid curves show the corresponding analytical results.